(Received 16 June 2026, Accepted 19 July 2026, Scheduled 29 July 2026)

Model Predictive Duty Cycle Control for Switched Reluctance Motors Based on Sliding Mode Compensation

Huiying Yu[1], Aide Xu[2,*], and Wanping Zhao[1]

[1] College of Electrical Engineering of Ships, Dalian Maritime University, Dalian 116026, China
[2] College of Information and Science Technology, Dalian Maritime University, Dalian 116026, China

ABSTRACT: In fixed switching frequency pulse-width modulation (PWM) drive systems for switched reluctance motors (SRMs), the duty cycle directly affects current-tracking precision and torque output performance. To address the slow dynamic response of conventional PI control and the model dependence and limited robustness of conventional model predictive duty-cycle control (MPDCC), this study proposes a robust duty-cycle control strategy based on double-power sliding mode compensation. This strategy constructs a duty-cycle generation mechanism by combining model predictive feedforward with sliding-mode compensation. It utilizes MPDCC to generate a base duty cycle, whereas a double-power sliding mode generates a compensation duty cycle to correct deviations. Simulated and experimental results demonstrate that the proposed strategy generates accurate PWM duty cycles, keeps the current tracking error bounded within a small quasi-sliding-mode band, and improves current-tracking accuracy and torque-ripple suppression under parameter-mismatch conditions, validating the robustness of the system against parameter mismatches.

1. INTRODUCTION

Switched reluctance motors (SRMs) have great potential in electric vehicle drives, aerospace, and industrial automation, owing to their robust structure, low cost, high fault tolerance, and suitability for high-temperature and high-speed operations [1, 2]. However, their doubly salient structure leads to highly saturated magnetic circuits and strongly nonlinear flux linkage characteristics, inevitably causing significant torque ripple and limiting their application in high-precision servo systems. Fixed-switching-frequency PWM has been widely adopted to suppress torque ripple and improve dynamic performance. This modulation approach imposes stringent requirements on the controller, demanding the precise generation of the PWM duty cycle to achieve accurate regulation of the phase voltage [3].

Traditional proportional-integral (PI) control is extensively used owing to its simple structure and easy implementation. Nevertheless, the inherent lag of integral action and bandwidth limitations of fixed gains make it prone to current-tracking lag and phase delay when confronted with the nonlinear inductance characteristics of the SRM. Consequently, achieving high-precision current tracking is challenging [4, 5]. To overcome these limitations, model predictive control (MPC) has received increasing attention. In [6], MPC was applied to an SRM drive system, where the current state was predicted using a discretized model, thereby significantly enhancing dynamic response speed. In [7], model predictive duty-cycle control (MPDCC) was proposed to inversely calculate the ideal duty cycle, effectively resolving the issue of unfixed switching frequencies inherent in conventional control schemes. However, MPC performance strongly depends on prediction model accuracy, and motor parameters inevitably vary due to magnetic saturation and temperature-induced resistance drift. Under parameter mismatch, the MPDCC exhibits deviations, resulting in static errors or dynamic lags in current tracking [8].

Sliding mode control (SMC) has been widely applied owing to its robustness, fast response, and simple structure. Existing SMC-based SRM control methods improve robustness and dynamic response by introducing improved reaching laws, adaptive mechanisms, neural networks, fuzzy compensators, or disturbance observers [9–13]. However, these methods often involve additional parameter tuning, training dependence, observer design, or structural coupling, which increases implementation complexity. Moreover, their applicability to fixed-switching-frequency duty-cycle generation under SRM parameter mismatch remains limited.

Existing robust MPC methods, such as tube-based MPC, disturbance-observer-based MPC, and adaptive MPC, can improve robustness, but they generally require invariant-set design, observer construction, or online parameter identification, increasing implementation complexity for SRM drives with nonlinear inductance characteristics. To address MPDCC performance degradation under parameter mismatch, this study proposes a robust MPDCC strategy based on double-power sliding-mode compensation. The MPDCC term generates the model-based base duty cycle, while the sliding-mode compensator produces an additional duty-cycle correction according to the current-tracking error. Thus, the proposed method preserves the prediction-based duty-cycle generation mechanism of MPDCC while improving robustness against duty-cycle deviations caused by model parameter mismatch.

* Corresponding author: Aide Xu (aidexu@dlmu.edu.cn).

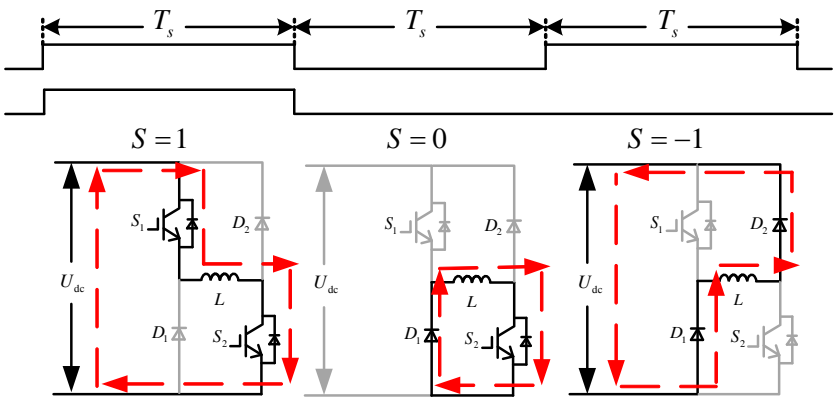

FIGURE 1. Relationship between PWM signals and the operating states of the power converter.

2. PRINCIPLE OF PWM DUTY CYCLE CONTROL

2.1. SRM Mathematical Model

Neglecting magnetic saturation and mutual inductance, the phase voltage equation of the SRM based on the minimum reluctance principle is given by

$$\begin{aligned} u_p &= R_s i_p + \frac{\mathrm{d}\psi_{\mathrm{p}}(\mathrm{i_p}, \theta)}{\mathrm{dt}} \\ &= R_s i_p + L_p(i_p, \theta)\frac{\mathrm{di_p}}{\mathrm{dt}} + e_p(i_p, \theta, \omega) \end{aligned} \tag{1}$$

where R_s is the phase resistance; i_p, ψ_p, θ, and ω represent the phase current, flux linkage, rotor position, and rotor speed; $L_p(i_p, \theta)$ is the incremental inductance; $e_p(i_p, \theta, \omega) = i_p\omega \cdot (\partial L_p/\partial\theta)$ is the back electromotive force of phase p.

The forward Euler method is adopted to discretize Eq. (1), and the discrete voltage model at time k can be obtained as follows:

$$u_p(k) = R_s i_p(k) + L_p(k)\frac{i_p(k+1) - i_p(k)}{T_s} + e_p(k) \tag{2}$$

Under ideal conditions, neglecting magnetic saturation and nonlinearities, the electromagnetic torque generated by the SRM is expressed as

$$T_e(k) = \frac{1}{2} i_p^2(k)\frac{\partial L_p(k)}{\partial\theta} \tag{3}$$

As indicated by (3), the electromagnetic torque is related to both the inductance-variation rate and the square of the phase current amplitude. Consequently, achieving high-performance torque control necessitates precise phase-current tracking.

2.2. Principle of PWM Duty Cycle Modulation

In an SRM drive system with a fixed switching frequency, the PWM maintains a constant switching period, T_s, and regulates the winding terminal voltage by adjusting the switch on time t_{on}. The duty cycle for the k-th period is defined as

$$D(k) = \frac{t_{on}}{T_s} \tag{4}$$

As shown in Fig. 1, PWM1 and PWM2 determine the operating states of the three-phase asymmetric converter. A high PWM output applies the DC bus voltage $+U_{\mathrm{dc}}$ to the winding, causing a rapid current rise, and the system is in the excitation state. Conversely, a low-PWM output yields an approximately zero voltage, resulting in a slow current decay, and the system enters the freewheeling state. At the turn-off angle, turning off all switches applies $-U_{\mathrm{dc}}$ to the winding, rapidly decreasing the current, and the system transitions to the demagnetization state.

To suppress the current ripple, soft-chopping control is typically adopted. The power converter alternately switches between the excitation ($S = 1$) and freewheeling ($S = 0$) states to achieve phase-current tracking. Within a fixed sampling period, a linear relationship exists between the duty cycle $D(k)$ and the average phase voltage $u_{\mathrm{avg}}(k)$, which is given by

$$u_{\mathrm{avg}}(k) = D(k) \cdot U_{\mathrm{dc}} \tag{5}$$

By neglecting the winding resistance voltage drop and substituting Eq. (1), the current derivative with respect to the duty cycle can be derived as Eq. (6), where U_{dc} is the DC bus voltage. Thus, accurate duty-cycle generation is essential for precise current tracking and overall system performance.

$$\frac{\Delta i}{\Delta t} \approx \frac{D(k) \cdot U_{\mathrm{dc}} - e_p(k)}{L_p(k)} \tag{6}$$

2.3. Conventional PI Duty Cycle Control and Its Limitations

Linear control strategies based on error feedback are commonly adopted to generate the PWM duty cycle for phase current tracking.

Based on the tracking error $e(k)$ between the reference current i_{ref} and the actual phase current $i_p(k)$, the PI controller generates the voltage reference through proportional and integral actions,

$$u_{\mathrm{PI}}(k) = K_p e(k) + K_i T_s \sum e(k) \tag{7}$$

where K_p and K_i are the proportional and integral gains, respectively. The final duty cycle D_{PI} generated by the PI con-

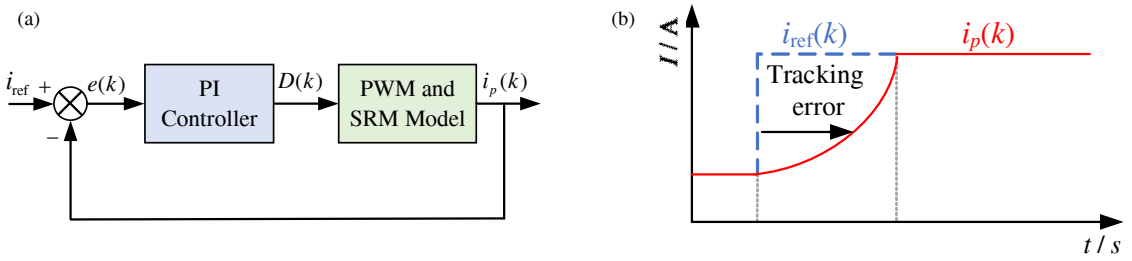

FIGURE 2. Conventional PI control structure and its dynamic response lag. (a) Block diagram of PI duty-cycle control and (b) dynamic response lag.

troller is given by (8), which satisfies $0 \leq D_{\mathrm{PI}} \leq 1$.

$$D_{\mathrm{PI}}(k) = \frac{u_{\mathrm{PI}}(k)}{U_{\mathrm{dc}}} \tag{8}$$

Although PI control can eliminate steady-state errors under steady-state conditions, it is inherently a lagging regulation mechanism based on error feedback, which limits its application in SRM current control. Fig. 2 illustrates the regulation mechanism of the PI controller and the issues regarding its dynamic performance. One primary issue is the dynamic phase lag in the current tracking. As shown in Fig. 2(b), when the reference current i_{ref} undergoes a sudden change, the actual current i_p cannot follow immediately owing to the impeding effects of the inductance and back-electromotive force e_p. Consequently, the controller must increase the duty cycle via the integral term to compensate for the error arising from the current deviation induced by e_p.

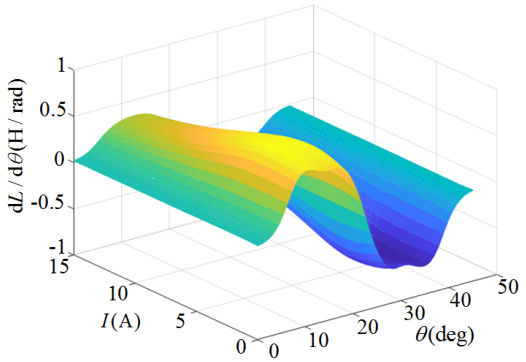

FIGURE 3. Nonlinear characteristic surface of the rate of change of inductance.

Furthermore, PI control exhibits poor adaptability to the SRM's nonlinear characteristics. As indicated in Fig. 3, inductance variation rate $\mathrm{d}L/\mathrm{d}\theta$ depends on rotor position and is also affected by magnetic saturation caused by phase current. Fixed gains K_p and K_i fail to simultaneously balance system stability and dynamic response speed. Therefore, PI control alone is insufficient for fast and precise phase-current tracking in SRM drives.

To overcome these limitations and achieve fast, precise phase-current tracking, advanced control strategies with active compensation and strong robustness are required.

3. DUTY CYCLE CONTROL STRATEGY WITH MODEL PREDICTIVE CONTROL AND SLIDING MODE COMPENSATION

To improve dynamic response and robustness, a composite duty-cycle control strategy, combining model predictive control (MPC) and sliding-mode compensation is proposed, as shown in Fig. 4. The final controller output $D(k)$ consists of the model-predicted duty cycle $D_0(k)$ and sliding-mode compensation duty cycle $D_1(k)$.

$$D(k) = D_0(k) + D_1(k) \tag{9}$$

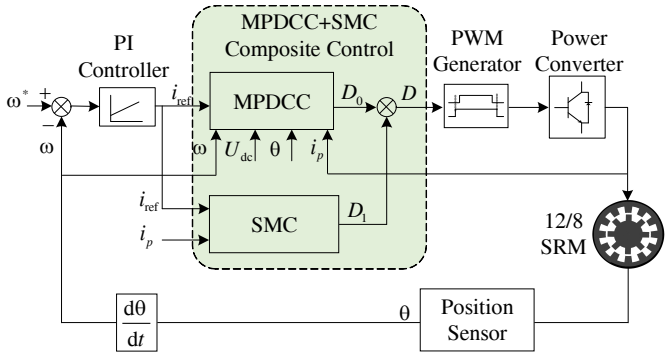

FIGURE 4. Block diagram of the composite duty-cycle control system with model predictive control and sliding mode compensation.

3.1. Duty Cycle Generation Strategy Based on Model Predictive Control

Based on the MPC concept and the discretized SRM voltage balance equation in Eq. (2), the predicted phase current at step $k+1$ is obtained as

$$i_p(k+1) = i_p(k) + \frac{T_s}{L_p(k)}[u_p(k) - R_s i_p(k) - e_p(k)] \tag{10}$$

To achieve fast current tracking, MPC forces $i_p(k+1)$ to reach the reference current within one sampling cycle. By substituting $i_p(k+1) = i_{\mathrm{ref}}(k)$, the ideal control voltage is obtained as

$$u_p^* = L_p(k)\frac{i_{\mathrm{ref}}(k) - i_p(k)}{T_s} + R_s i_p(k) + e_p(k) \tag{11}$$

Consequently, the MPC-based duty cycle is derived as Eq. (12). Theoretically, with accurate motor parameters, this

strategy can eliminate the current error within one control period.

$$D_0(k)=\frac{u_p^*}{U_{\rm dc}}=\frac{1}{U_{\rm dc}}\left(L_p(k)\frac{i_{\rm ref}(k)-i_p(k)}{T_s}+R_s i_p(k)+e_p(k)\right) \quad (12)$$

In practice, the inductance and back-EMF of SRMs are highly nonlinear. The controller usually uses the offline inductance $L_{\rm n}$ obtained from standstill tests, which differs from the actual inductance $L_{\rm r}$. To describe this mismatch, a local equivalent factor is introduced as

$$\eta(i,\theta)=\frac{L_n(i,\theta)}{L_r(i,\theta)} \quad (13)$$

When the current varies with load, $\eta(i,\theta)$ may also change. For simplicity, $\eta(i,\theta)$ is denoted as η in the following local analysis. Using this local equivalent mismatch factor, the relationship between the MPDCC duty cycle and the ideal duty cycle can be approximated as

$$\begin{aligned} D_0(k) &\approx \frac{L_n(k)}{U_{\rm dc}}\frac{i_{\rm ref}(k)-i_p(k)}{T_s} \\ &= \eta\cdot\frac{L_r(k)}{U_{\rm dc}}\frac{i_{\rm ref}(k)-i_p(k)}{T_s}=\eta\cdot D_{\rm ref}(k) \end{aligned} \quad (14)$$

This approximation reveals how inductance mismatch affects MPDCC duty-cycle calculation. The variation of $\eta(i,\theta)$ over a wider operating range is treated as bounded model uncertainty and compensated by the sliding mode strategy introduced in the next subsection.

According to Eq. (14), when $\eta<1$, the MPC-generated duty cycle is insufficient, resulting in inadequate excitation voltage, poor current tracking, and steady state error. When $\eta>1$, the excessive duty cycle causes current overshoot. Therefore, a sliding-mode compensator is introduced to suppress the adverse effects of parameter uncertainty.

3.2. Compensation Duty Cycle Generation Strategy Based on Sliding Mode Control

A linear sliding surface is adopted, with the current tracking error selected as the state variable:

$$s(k)=e(k)=i_{\rm ref}(k)-i_p(k) \quad (15)$$

To suppress the current tracking error, the system drives $s(k)$ to the sliding surface $s(k)=0$ within finite time and then maintains sliding motion. As shown in Fig. 5, the trajectory includes a reaching phase and a sliding phase.

The reaching law determines both convergence speed and chattering amplitude. Since the conventional exponential reaching law cannot effectively balance fast convergence and chattering suppression, a discrete double-power reaching law is adopted:

$$\begin{aligned} s(k+1)-s(k) &= -\frac{T_s}{L_p(k)}\Big[\alpha\,|s(k)|^{\lambda_1}\,\mathrm{sgn}\,(s(k)) \\ &\quad +\beta\,|s(k)|^{\lambda_2}\,\mathrm{sgn}\,(s(k))\Big] \end{aligned} \quad (16)$$

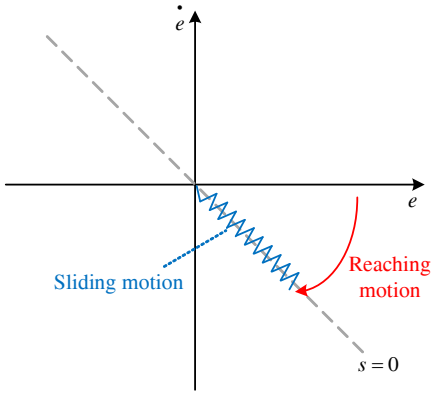

FIGURE 5. State trajectory of sliding-mode control.

where $s(k)$ is the discrete sliding surface; $\alpha>0$, $\beta>0$ are the reaching gains; $\lambda_1>1$ is the fast power coefficient; and $0<\lambda_2<1$ is the convergence power coefficient. By combining the two power terms, this reaching law enables rapid convergence when the state is far from the sliding surface and reduces the reaching speed near the surface, achieving both fast dynamic response and system stability.

Based on (9), the discrete current predictive model for the SRM is derived as

$$\begin{aligned} i_p(k+1) &= i_p(k)+\frac{T_s}{L_p(k)}\Big[\Big(D_0(k)+D_1(k)\Big)U_{\rm dc} \\ &\quad -R_s i_p(k)-e_p(k)\Big] \end{aligned} \quad (17)$$

Assuming that $i_{\rm ref}(k+1)\approx i_{\rm ref}(k)$, rearranging the equation yields the system state equation as (18),

$$s(k+1)=s(k)-\frac{T_s U_{\rm dc}}{L_p(k)}D_1(k)+d(k) \quad (18)$$

where $d(k)$ denotes the uncertainty term, mainly caused by model parameter mismatch and MPC duty-cycle calculation errors. Since $d(k)$ is unknown in practice, it is not directly included in the control law. By matching the controllable part of Eq. (18) with the reaching law in Eq. (16), the nominal compensation duty cycle is designed as

$$D_1(k)=\frac{1}{U_{\rm dc}}\left[\alpha\,|s(k)|^{\lambda_1}\mathrm{sgn}(s(k))+\beta\,|s(k)|^{\lambda_2}\mathrm{sgn}(s(k))\right] \quad (19)$$

The MPDCC term $D_0(k)$ provides the model-based base duty cycle, and the SMC term $D_1(k)$ serves as an independent feedback compensation term to correct the residual duty-cycle error caused by parameter mismatch. Since $D_1(k)$ is generated from the current tracking error and the DC bus voltage, it is independent of motor parameters such as inductance, winding resistance, and back-EMF. Under parameter mismatch conditions, $D_1(k)$ is superimposed on $D_0(k)$, driving the current tracking error into a small quasi-sliding-mode band.

To avoid duty-cycle saturation, an anti-windup-like limiter is applied to $D_1(k)$. The compensation duty cycle is constrained by the remaining margin after D0(k), ensuring $0\le D(k)=D_0(k)+D_1(k)\le 1$ and preventing windup-like oscillation between the MPDCC feedforward and SMC feedback terms.

3.3. Stability Proof

To analyze the practical stability of the proposed strategy under parameter mismatch and unknown disturbances, a discrete-time Lyapunov stability proof is conducted. The Lyapunov function is selected as

$$V(k) = \frac{1}{2}s^2(k) \tag{20}$$

The first-order difference is

$$\begin{aligned}\Delta V(k) &= \frac{1}{2}\left[s^2(k+1) - s^2(k)\right] \\ &= \frac{1}{2}\left[s(k+1) - s(k)\right] \cdot \left[s(k+1) + s(k)\right]\end{aligned} \tag{21}$$

To simplify the notation, define

$$H(k) = \alpha \left|s(k)\right|^{\lambda_1} + \beta \left|s(k)\right|^{\lambda_2} \tag{22}$$

Then, Eq. (16) can be rewritten as

$$s(k+1) = s(k) - \frac{T_s}{L_p(k)}H(k)\mathrm{sgn}(s(k)) \tag{23}$$

substituting Eq. (23) into Eq. (21) yields

$$\Delta V(k) = -\frac{T_s}{L_p(k)}H(k)\left|s(k)\right| + \frac{1}{2}\left[\frac{T_s}{L_p(k)}H(k)\right]^2 \tag{24}$$

According to the discrete-time Lyapunov criterion, $\Delta V(k) < 0$ should hold outside the boundary layer, i.e., $|s(k)| > \varepsilon$. Since $T_s > 0, L_p(k) > 0, \alpha > 0, \beta > 0$, and $H(k) > 0$ for $s(k) \neq 0$, Eq. (24) gives the stability condition

$$\frac{T_s}{L_p(k)}H(k) < 2\left|s(k)\right| \tag{25}$$

Equivalently, the sampling period should satisfy,

$$T_s < \frac{2L_p(k)}{\alpha\left|s(k)\right|^{\lambda_1 - 1} + \beta\left|s(k)\right|^{\lambda_2 - 1}} \tag{26}$$

Since $0 < \lambda_2 < 1$, $|s(k)|^{\lambda_2 - 1}$ becomes unbounded as $|s(k)|$ approaches zero. Therefore, a boundary layer $\varepsilon > 0$ is introduced, and the stability analysis is performed for $|s(k)| > \varepsilon$. Assuming $L_p(k) \geq L_{\min} > 0$ and $|s(k)| \leq s_{\max}$, for $|s(k)| > \varepsilon$, one has $|s(k)|^{\lambda_1 - 1} \leq s_{\max}^{\lambda_1 - 1}$ and $|s(k)|^{\lambda_2 - 1} < \varepsilon^{\lambda_2 - 1}$. Thus, a conservative sufficient condition is obtained as

$$T_s < \frac{2L_{\min}}{\alpha s_{\max}^{\lambda_1 - 1} + \beta\varepsilon^{\lambda_2 - 1}} \tag{27}$$

When Eq. (27) is satisfied, the Lyapunov function decreases monotonically outside the boundary layer, and the current tracking error is driven into the quasi-sliding-mode band $|s(k)| \leq \varepsilon$. Within this band, strict convergence to $s(k) = 0$ is not required, which avoids chattering amplification caused by sampling noise, PWM discretization, and current measurement uncertainty. Thus, the proposed controller guarantees practical stability under bounded parameter mismatch and disturbance, provided that the compensation duty cycle remains within the available duty-cycle margin.

In practical PWM drive systems, T_s is usually fixed, so Eq. (27) serves as a parameter selection guideline. Since $s(k) = i_{\mathrm{ref}}(k) - i_p(k)$, ε denotes the allowable current tracking error band. A larger ε reduces chattering but increases steady-state error, whereas a smaller ε improves accuracy but increases sensitivity to measurement noise and PWM discretization. After ε is selected, the reaching-law gains are tuned according to Eq. (27), while avoiding excessive chattering and duty-cycle saturation.

4. RESULTS ANALYSIS

To verify the effectiveness of the proposed strategy, an SRM drive simulation model was built in MATLAB/Simulink, and experiments were conducted on a 12/8-pole SRM platform. The motor parameters are presented in Table 1.

TABLE 1. Motor parameters.

Parameter name	Parameter value
Stator/rotor poles	12/8
Rated Power	5.5 kW
Rated torque	30 N·m
Rated speed	1500 r/min
Stator resistance	1.472 Ω

4.1. Simulation Analysis

To verify the superiority of the proposed MPDCC + SMC composite control strategy over the traditional PI duty-cycle control under ideal matched conditions, the reference speed and load torque were set to 500 r/min and 5 N·m, respectively, with $\theta_{\mathrm{on}} = 2°$ and $\theta_{\mathrm{off}} = 20°$. The obtained simulation waveforms are shown in Fig. 6.

As shown in Fig. 6, the phase current controlled by the conventional PI controller fails to rise quickly to the reference value and cannot maintain a stable flat profile. Conversely, the proposed MPDCC + SMC method enables the current to rapidly reach the reference, eliminates the current dip, and closely follows the reference waveform, demonstrating faster and more accurate phase-current tracking. Furthermore, the torque ripple is reduced from 73.0% with the traditional method to 46.9% with the proposed method, verifying its effectiveness in torque ripple suppression.

When other operating conditions remained unchanged, the waveforms when the reference speed was increased to 800 r/min are presented in Fig. 7. The proposed strategy was still capable of tracking the reference current precisely and quickly while successfully mitigating torque ripple.

To verify the independent effectiveness of the SMC compensator, standalone MPDCC and the proposed MPDCC + SMC method were compared under the same parameter-mismatch condition. Fig. 8 shows the simulation waveforms at 500 r/min and 10 N·m. For the double-power reaching law, the power co-

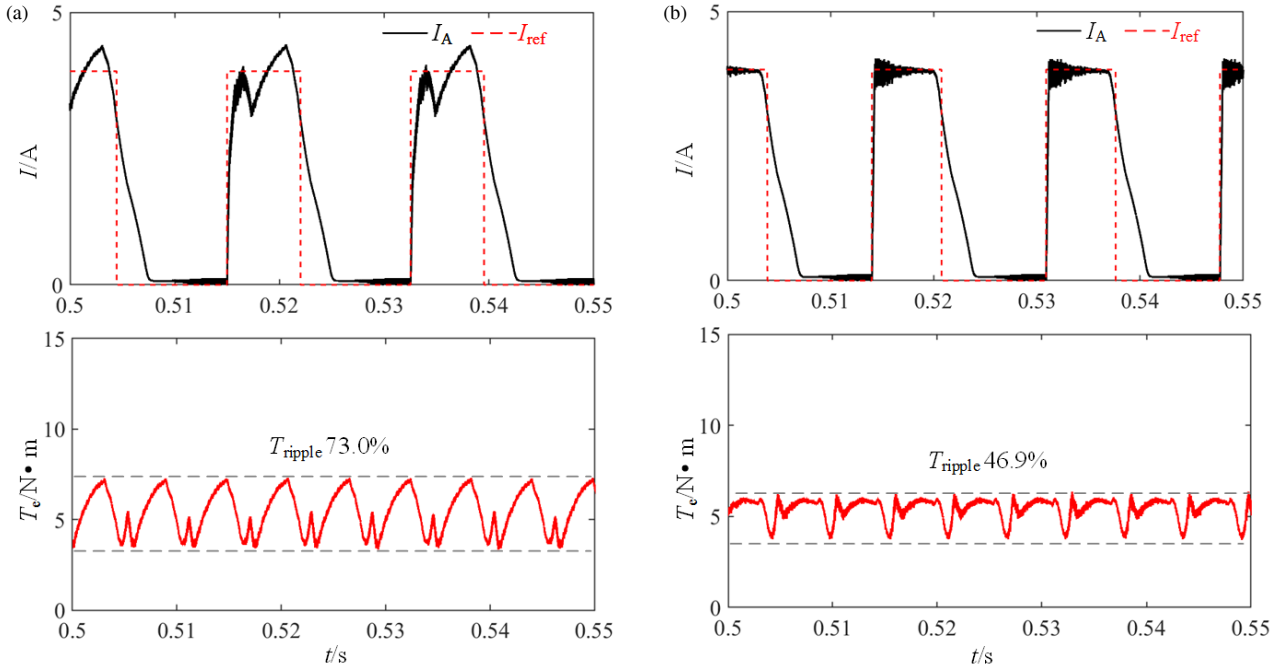

FIGURE 6. Torque and current tracking waveforms under ideal conditions at 500 r/min and 5 N·m. (a) PI. (b) MPDCC + SMC.

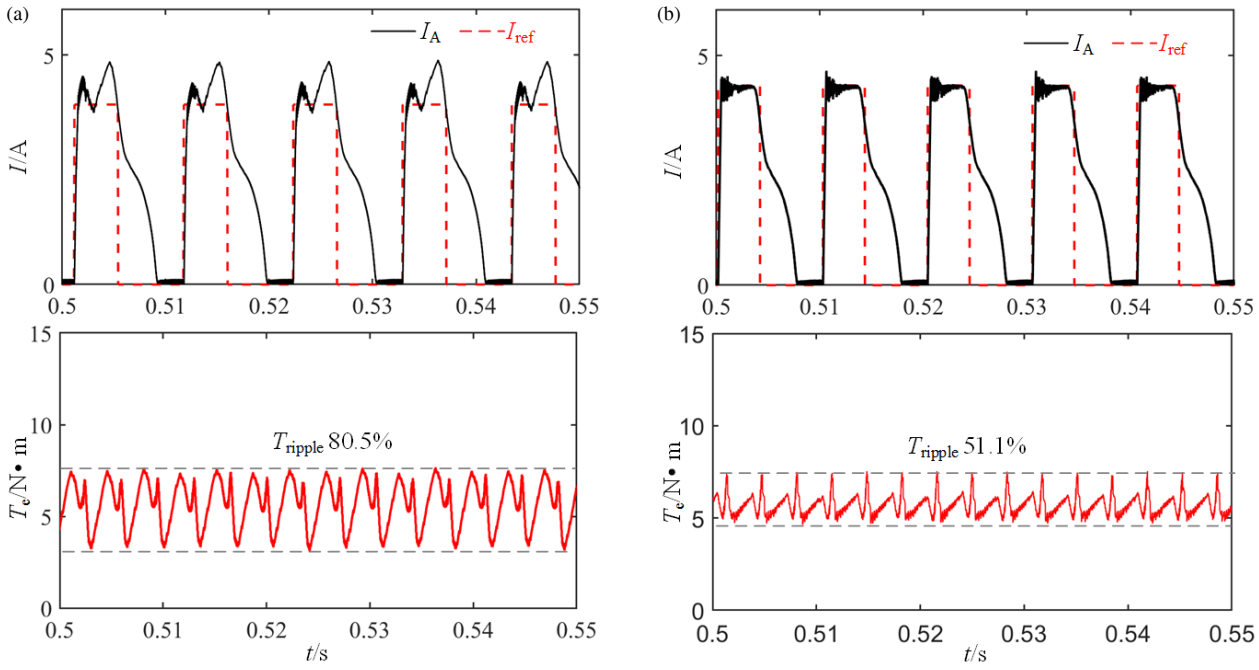

FIGURE 7. Torque and current tracking waveforms under ideal conditions at 800 r/min and 5 N·m. (a) PI. (b) MPDCC + SMC.

efficients were set to $\lambda_1 = 1.5$ and $\lambda_2 = 0.4$, and the reaching gains were $\alpha = 3.0 \times 10^6$ and $\beta = 1.0 \times 10^6$.

As shown in Fig. 8(a), due to the model parameter mismatch, the duty cycle calculated by the MPC was excessively small, preventing the actual current from tracking the reference and causing triangular waveform distortion. This leads to excessive torque ripple, with the torque ripple coefficient reaching 96.6%. Fig. 8(b) displays the waveforms after the introduction of sliding-mode compensation. The SMC rapidly responds to the current tracking error and generates the corresponding compensation duty cycle. This enables the phase current to quickly track the reference value and restore its square-wave characteristics, and the torque ripple coefficient is 47.3%. Since both methods share the same MPDCC feedforward term, the reduction from 96.6% to 47.3% confirms the independent compensation effect of the SMC term.

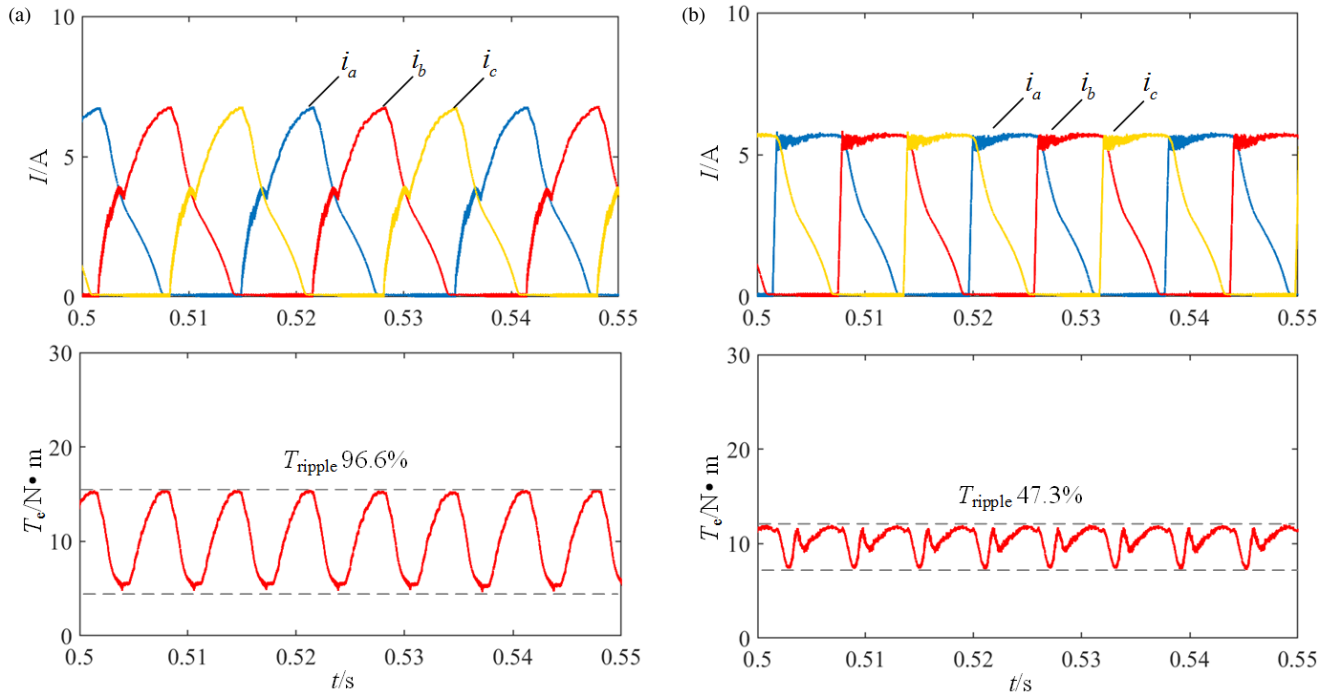

FIGURE 8. Torque and current tracking waveforms under parameter mismatch at 500 r/min and 10 N·m. (a) MPDCC and (b) MPDCC + SMC.

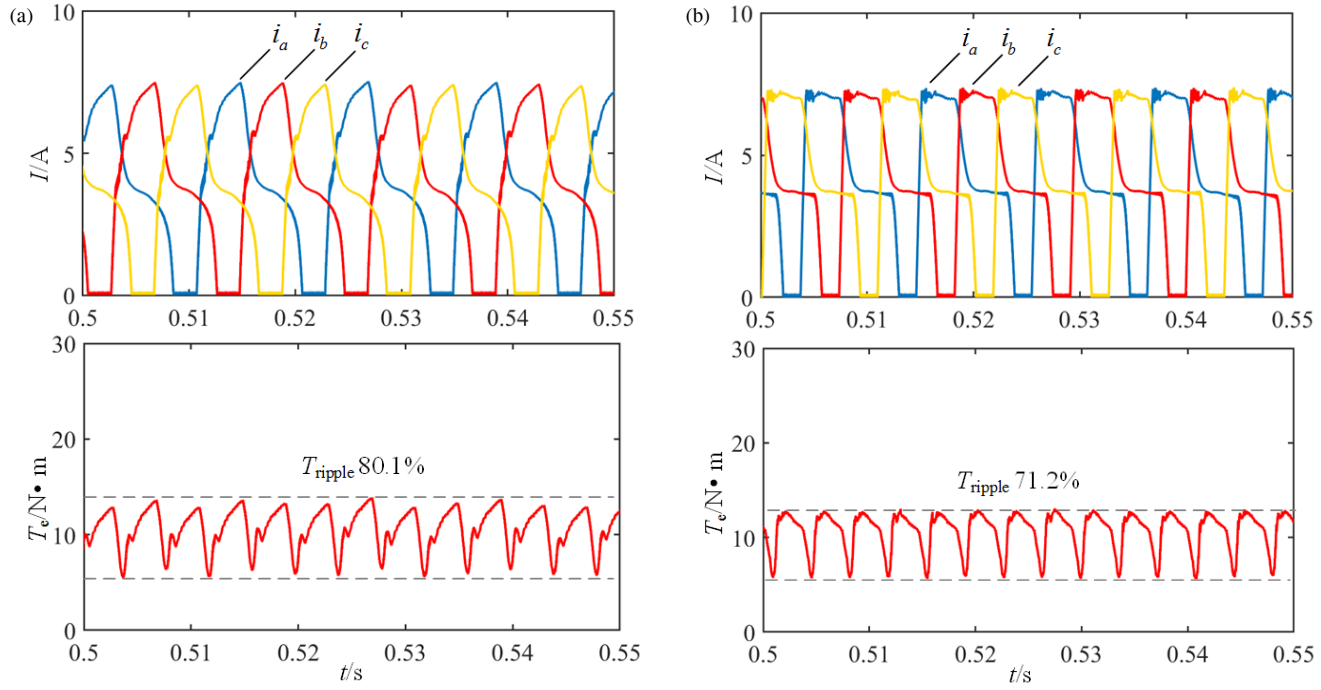

FIGURE 9. Torque and current tracking waveforms under parameter mismatch at 800 r/min and 10 N·m. (a) MPDCC and (b) MPDCC + SMC.

Figure 9 shows the simulation results when the speed is increased to 800 r/min, further demonstrating that the proposed strategy still outperforms MPDCC at this speed.

In summary, the quantitative indicators in Table 2 demonstrate that the proposed MPDCC + SMC strategy consistently yields lower torque ripples across a wide speed range than conventional methods. Even under severe inductance mismatch and high-speed operation, the double-power sliding mode mechanism enables rapid error compensation, improving current tracking and torque ripple suppression.

TABLE 2. Performance and torque ripple quantitative comparison under diverse operating conditions.

Operating Condition	Speed-Load	Baseline Strategy (T_{ripple})	Proposed (T_{ripple})	Reduction (Δ)
Ideal	500 r/min, 5 N· m	73.0% (PI)	46.9% (MPDCC + SMC)	26.1%
	800 r/min, 5 N· m	80.5% (PI)	51.1% (MPDCC + SMC)	29.4%
Mismatch	500 r/min, 10 N· m	96.6% (MPDCC)	47.3% (MPDCC + SMC)	49.3%
	800 r/min, 10 N· m	80.1% (MPDCC)	71.2% (MPDCC + SMC)	8.9%

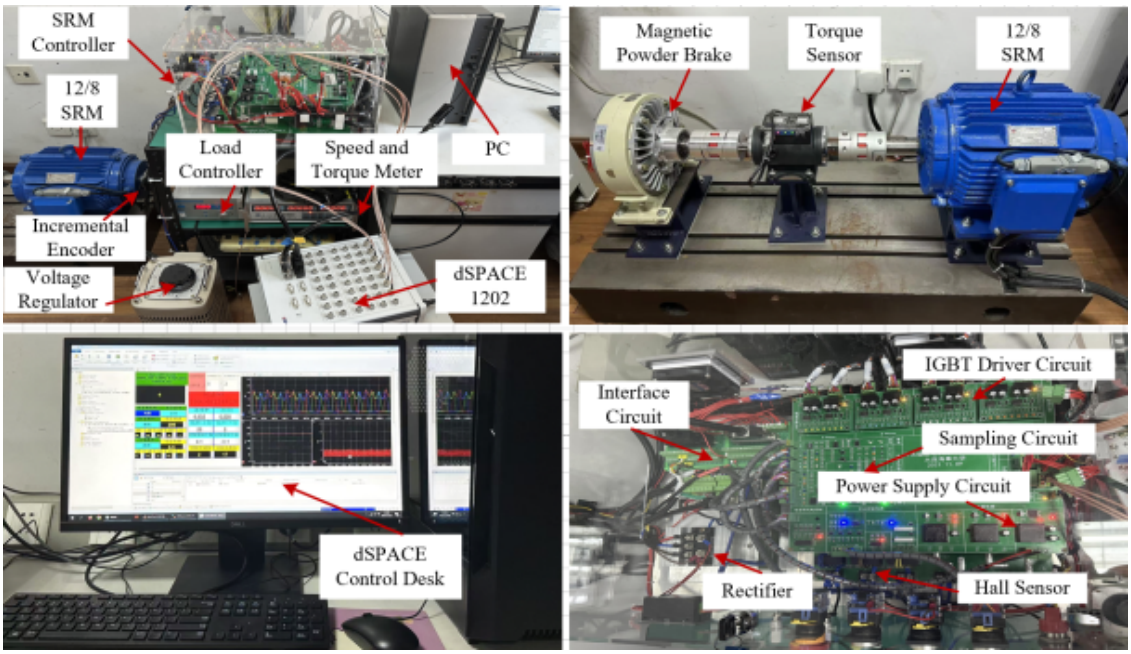

FIGURE 10. Experimental platforms.

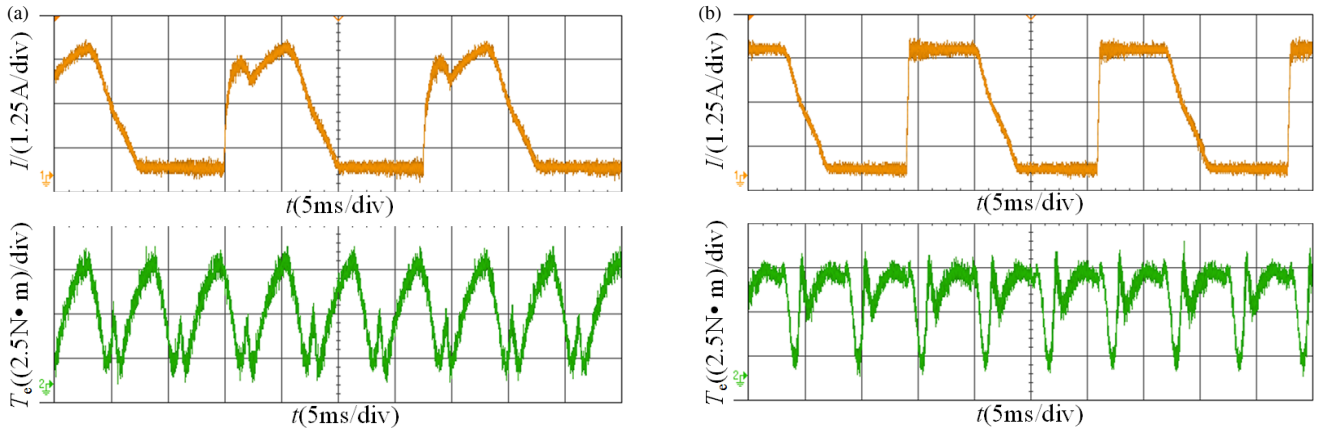

FIGURE 11. Experimental comparison results of current and torque waveforms under ideal conditions at 500 r/min and 5 N·m. (a) PI and (b) MPDCC + SMC.

4.2. Experimental Analysis

Figure 10 shows the three-phase 12/8 SRM experimental platform, which consists mainly of an SRM controller, a 12/8 SRM, a dSPACE control platform, and a host computer. The controller comprises a power converter, voltage and current sensors, and isolated gate driver circuits. The control algorithm was implemented on a dSPACE MicroLabBox 1202 real-time HIL system. Different load torque conditions were achieved by adjusting the excitation current of the magnetic powder brake.

Figure 11 shows the experimental waveforms under ideal conditions without parameter mismatch, namely 500 r/min and 5 N·m. The PI-controlled phase current exhibits obvious wave-

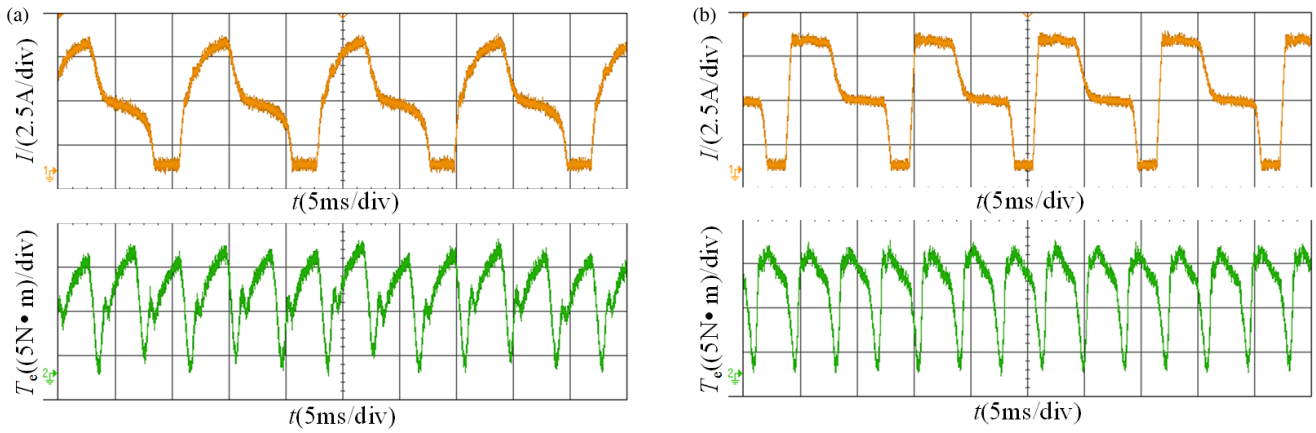

FIGURE 12. Experimental comparison results of current and torque waveforms under parameter mismatch at 800 r/min and 10 N·m. (a) MPDCC and (b) MPDCC + SMC.

form distortion, with a torque ripple of approximately 78.3%. In contrast, the proposed strategy maintains a smoother flat-top current waveform and effectively suppresses the torque ripple, reducing it by approximately 25.1 percentage points. This demonstrates the superior current tracking and torque ripple suppression of the proposed method.

Figure 12 presents the experimental results under parameter mismatch at 800 r/min and 10 N·m. At higher speeds, parameter mismatch has a more pronounced effect on prediction accuracy. Under the MPDCC strategy, the phase current shows noticeable distortion, leading to degraded torque performance. By contrast, the proposed MPDCC + SMC method maintains satisfactory current regulation performance even at higher operating speeds. The phase-current waveform closely follows the reference current, whereas the corresponding torque waveform becomes significantly smoother. These results demonstrate that the proposed control strategy effectively mitigates parameter mismatch effect and maintains stable control performance over a wider speed range.

For quantitative comparison, Fig. 11 shows that the torque ripple coefficient is approximately 78.3% for the PI controller and 53.2% for the proposed MPDCC + SMC method, corresponding to a reduction of 25.1 percentage points. In the parameter-mismatch experiment shown in Fig. 12, the torque ripple coefficients of MPDCC and MPDCC + SMC are 85.7% and 74.4%, respectively.

5. CONCLUSION

This study proposes an MPDCC + SMC composite duty-cycle control strategy with a discrete double-power reaching law for SRM drives. The MPDCC term provides the model-based base duty cycle, while the SMC term compensates for residual duty-cycle errors caused by parameter mismatch. Theoretical analysis proves that the current tracking error can be bounded within a quasi-sliding-mode band under the derived stability condition. Simulated and experimental results show that the proposed strategy improves current tracking, suppresses torque ripple, and maintains robustness under inductance mismatch and high-speed operation compared with conventional PI control and standalone MPDCC.

REFERENCES

[1] Cheng, H., D. Zhang, S. Liao, D. Shao, and Y. Hu, "Integrated drive converter of SDS-SRM with isolation and nonisolation charging capabilities for electric vehicle," *IEEE Transactions on Industrial Electronics*, Vol. 69, No. 9, 8679–8691, 2022.

[2] Sree, P. B. and N. P. G. Bhavani, "Efficiency improvement of electrical vehicles using novel switched reluctance motor and compared with permanent magnet motor by reducing power loss," in *2023 6th International Conference on Contemporary Computing and Informatics (IC3I)*, Vol. 6, 1473–1477, Gautam Buddha Nagar, India, 2023.

[3] Scalcon, F. P., G. Fang, C. J. V. Filho, H. A. Gründling, R. P. Vieira, and B. Nahid-Mobarakeh, "A PWM fixed-gain super-twisting sliding mode current controller for switched reluctance motors," in *IECON 2022 — 48th Annual Conference of the IEEE Industrial Electronics Society*, 1–6, Brussels, Belgium, 2022.

[4] Wang, X., Y. Niazi, S. Tavakolian, A. Gholaminejad, G. Fang, S. Dhale, D. F. Valencia, B. Nahid-Mobarakeh, and A. Emadi, "A review of current control strategies for switched reluctance motor drives: Performance evaluation across a wide speed range," *IEEE Open Journal of the Industrial Electronics Society*, Vol. 7, 136–156, 2026.

[5] Ahmad, S. S., M. Thirumalasetty, and G. Narayanan, "Predictive current control of switched reluctance machine for accurate current tracking to enhance torque performance," *IEEE Transactions on Industry Applications*, Vol. 60, No. 1, 1837–1848, 2024.

[6] Li, W., Z. Cui, S. Ding, F. Chen, and Y. Guo, "Model predictive direct torque control of switched reluctance motors for low-speed operation," *IEEE Transactions on Energy Conversion*, Vol. 37, No. 2, 1406–1415, 2022.

[7] Yang, Y. and J. Shao, "A predictive current control strategy for switched reluctance motor with sector division and duty cycle calculation," in *2025 5th International Conference on Mechanical, Electronics and Electrical and Automation Control (METMS)*, 908–912, Chongqing, China, 2025.

[8] Fu, R., "Robust model predictive flux control of pmsm drive using a compensated stator flux predictor," *IEEE Access*, Vol. 9, 136 736–136 743, 2021.

[9] Han, Z. and X. Li, "Improved adaptive sliding node control strategy for switched reluctance motors," in *2025 5th International Conference on New Energy and Power Engineering (ICNEPE)*, 1017–1021, Guangzhou, China, 2025.

[10] Wang, L., J. Zhang, X. Xu, and G. Liu, "Direct instantaneous torque control of switched reluctance motors with improved reaching law adaptive sliding mode control," in *2023 3rd International Conference on Electrical Engineering and Mechatronics Technology (ICEEMT)*, 581–586, Nanjing, China, 2023.

[11] Wang, S.-Y., F.-Y. Liu, and J.-H. Chou, "Design on sliding mode controller with adaptive fuzzy compensation for switched reluctance motor drive systems," in *2016 International Symposium on Computer, Consumer and Control (IS3C)*, 239–242, Xi'an, China, 2016.

[12] Dai, W., H. Shan, and H. Ma, "Doubly salient electromagnetic generator based on PID sliding mode control with constant switching frequency," *Alexandria Engineering Journal*, Vol. 118, 384–392, 2025.

[13] Ren, P., J. W. Zhu, Y. Zhao, Y. P. Liu, Z. Jing, and S. K. Zhang, "Speed control strategy for switched reluctance motor based on dual sliding mode controller," *Proceedings of the CSEE*, Vol. 44, No. 11, 4501–4513, 2024.